ADVANCED MATERIALS
www.advmat.de

Colossal Magnetoresistance without Mixed Valence in a Layered Phosphide Crystal

*Zhi-Cheng Wang, Jared D. Rogers, Xiaohan Yao, Renee Nichols, Kemal Atay, Bochao Xu, Jacob Franklin, Ilya Sochnikov, Philip J. Ryan, Daniel Haskel, and Fazel Tafti**

Materials with strong magnetoresistive responses are the backbone of spintronic technology, magnetic sensors, and hard drives. Among them, manganese oxides with a mixed valence and a cubic perovskite structure stand out due to their colossal magnetoresistance (CMR). A double exchange interaction underlies the CMR in manganates, whereby charge transport is enhanced when the spins on neighboring Mn^{3+} and Mn^{4+} ions are parallel. Prior efforts to find different materials or mechanisms for CMR resulted in a much smaller effect. Here an enormous CMR at low temperatures in $EuCd_2P_2$ without manganese, oxygen, mixed valence, or cubic perovskite structure is shown. $EuCd_2P_2$ has a layered trigonal lattice and exhibits antiferromagnetic ordering at 11 K. The magnitude of CMR (10^4%) in as-grown crystals of $EuCd_2P_2$ rivals the magnitude in optimized thin films of manganates. The magnetization, transport, and synchrotron X-ray data suggest that strong magnetic fluctuations are responsible for this phenomenon. The realization of CMR at low temperatures without heterovalency leads to a new regime for materials and technologies related to antiferromagnetic spintronics.

Colossal magnetoresistance (CMR) has been a subject of intense research due to its central place in the physics of correlated electron systems as well as its relevance to magnetic memory and sensing technologies.[1–3] The accepted paradigm of CMR is based on the manganate perovskite materials where a mixed valence of Mn^{3+}/Mn^{4+} mediates a ferromagnetic double-exchange (DE) interaction and a structural Jahn–Teller (JT) distortion, which cooperatively lead to a phase transition from paramagnetic insulator to ferromagnetic (FM) metal.[4–9] As a result, the electrical resistivity shows a peak near the Curie temperature (T_C) which rapidly drops in response to an external magnetic field, leading to a large negative magnetoresistance known as CMR.[4,10] It has remained a challenge in materials science to deviate from this paradigm and produce a sizable CMR either near an antiferromagnetic (AFM) transition or in materials without manganese, DE interaction, and JT distortion.[11–14] Overcoming this challenge is motivated by a surge of interest in the AFM spintronic and quantum information technologies that call for new materials and mechanisms of CMR based on AFM ordering at lower temperatures.[15–18]

In this communication, we report the striking observation of an enormous CMR in $EuCd_2P_2$, a material which is devoid of all traditional components of CMR. $EuCd_2P_2$ does not have manganese, oxygen, a mixed valence, a DE interaction, a perovskite structure, or a JT distortion. It has an AFM order at low temperature (T_N = 11 K), instead of the FM order at high temperature as seen in manganates. It has a trigonal unit cell with alternating layers of edge-shared EuP_6 octahedra and CdP_4 tetrahedra, different from the cubic lattice of manganates. We will show that strong magnetic fluctuations within the layered structure of this material provide a new mechanism for CMR that is aligned with the current progress in AFM spintronics.

A typical in-plane resistivity curve $\rho_{ab}(T)$ from a $EuCd_2P_2$ single crystal reveals a large peak at 18 K in zero magnetic field (**Figure 1**a). The peak drops by six-fold at only 0.5 T and by 46-fold at 5 T. Inset of Figure 1a shows that $\rho(T)$ fits to a bad metal behavior[19] where the high-temperature resistivity and even the residual resistivity (ρ_0 = 12.6 mΩ cm) are well above the Ioffe-Regel limit (1 mΩ cm). In fact, the resistivity barely changes with temperature and the residual resistivity ratio (RRR = R_{300K}/R_0) is only 1.9. We highlight three temperature regimes in the inset of Figure 1a: an initial poor metallic regime at high temperatures in yellow, an intermediate regime in red with CMR due to magnetic fluctuations (discussed below), and a blue region at low temperatures where the AFM order sets in

Dr. Z.-C. Wang, J. D. Rogers, X. Yao, R. Nichols, K. Atay, Prof. F. Tafti
Departments of Physics
Boston College
140 Commonwealth Avenue, Chestnut Hill, MA 02467, USA
E-mail: fazel.tafti@bc.edu
B. Xu, J. Franklin, Prof. I. Sochnikov
Physics Department
University of Connecticut
Storrs, CT 06269, USA
Prof. I. Sochnikov
Institute of Material Science
University of Connecticut
Storrs, CT 06269, USA
Dr. P. J. Ryan, Dr. D. Haskel
Advanced Photon Source
Argonne National Laboratory
Argonne, IL 60439, USA
Dr. P. J. Ryan
School of Physical Sciences
Dublin City University
Dublin 9 D09 V209, Ireland
The ORCID identification number(s) for the author(s) of this article can be found under https://doi.org/10.1002/adma.202005755.

DOI: 10.1002/adma.202005755

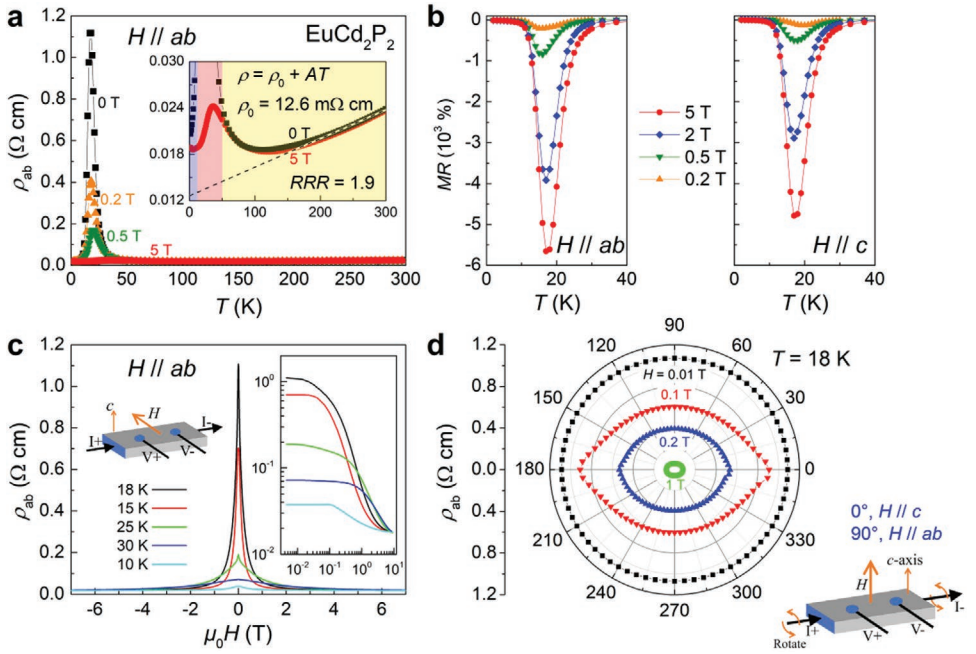

Figure 1. a) Temperature dependence of resistivity at several fields. The dashed line in the inset is a linear fit to extract the residual resistivity from the zero-field data (black squares). b) Magnetoresistance in a narrow temperature range in both in-plane and out-of-plane field directions. c) Field dependence of resistivity at several temperatures. Inset shows two orders of magnitude drop in resistivity in less than 4 T. d) Angle dependence of resistivity at several fields, showing a mild anisotropy. The 0° and 90° correspond to $H\|c$ and $H\|ab$, respectively.

and CMR disappears. Note that unlike the manganates,[10] the resistivity of $EuCd_2P_2$ remains much larger than 1 mΩ cm even at the lowest temperatures.

We define magnetoresistance as MR = 100% × $(R_H - R_0)/R_H$ and plot it as a function of temperature at a few representative fields in Figure 1b. The magnitude of MR exceeds -10^3% in less than 1 T regardless of the field direction. For comparison, MR in single crystals of $La_{0.75}Ca_{0.25}MnO_3$, the archetypal manganate material, is only –25% at 1 T and –400% at 4 T with the same definition of magnetoresistance.[10] It reaches -10^3% in epitaxially grown thin films of $La_{0.67}Ca_{0.33}MnO_3$ or $La_{0.60}Y_{0.07}Ca_{0.33}MnO_x$, and can be as high as -10^{4-5}% after optimizing the oxygen content.[20–22] It is remarkable that as-grown crystals of $EuCd_2P_2$, without any material optimization, can exhibit a truly colossal effect. This will be later enhanced when we examine the effect of current direction on CMR and find a staggering -10^4% MR when the current is out-of-plane instead of in-plane (ρ_c instead of ρ_{ab}).

Both the temperature and field dependence of CMR are extremely sharp in $EuCd_2P_2$, making it a good material for the low-temperature magnetic sensing and read/write devices.[16] Figure 1c shows that the field dependence of resistivity has a distinct Lorentzian peak shape with a narrow full-width at half-maximum (FWHM) of 0.38 T at 18 K (see also Figure S1, Supporting Information). Note that CMR maximizes at 18 K which is $1.5T_N$. It becomes negligible below T_N and above $5T_N$, that is, outside the temperature regime of magnetic fluctuations (insets of Figure 1a,c).

The CMR behavior in $EuCd_2P_2$ is nearly independent of the field direction, as seen in the 360° scan of the resistivity at 18 K in Figure 1d. There is no discernible angular dependence in ρ(18 K) at a small field of 100 Oe, and the maximum anisotropy is only a factor of 1.5 at H = 0.1 T. Furthermore, the CMR does not change by changing the in-plane current direction (Figure S2, Supporting Information); however, it increases by one order of magnitude when the current direction is changed from in-plane to out-of-plane as will be seen later.

To investigate the underlying mechanism of CMR in $EuCd_2P_2$, we measured magnetization as a function of temperature and field in both the in-plane and out-of-plane directions. It is helpful to examine the crystal structure before discussing the magnetic data. **Figure 2**a shows the trigonal lattice of $EuCd_2P_2$ in space group $P\bar{3}m1$ with alternating Eu and Cd layers (see X-ray analysis in Figure S3, Supporting Information. The individual layers are triangular networks of either edge-shared EuP_6 octahedra or CdP_4 tetrahedra. We show one magnetic unit cell in Figure 2a where the order is FM within the Eu layers but with alternating direction (AFM) between the layers. This A-type AFM order has been previously reported in crystals of $EuCd_2As_2$ and $EuCd_2Sb_2$,[23–27] and is consistent with the magnetic susceptibility data in Figure 2b that shows a FM order when $H\|ab$, but an AFM order when $H\|c$. The finite residual $\chi_c(T)$ near zero temperature indicates a small out-of-plane spin canting superposed on the A-type AFM order. At low temperatures, the in-plane susceptibility (black data) is 10 times larger than the out-of-plane one (red data), suggesting a strong magnetocrystalline anisotropy. This is confirmed in Figure 2c where the saturation field for the in-plane $M(H)$ curve (0.16 T) is 10 times smaller than the out-of-plane $M(H)$ curve (1.6 T). Thus, $EuCd_2P_2$ has a significant easy-plane anisotropy consistent with its layered structure. Inset of Figure 2b indicates T_N = 11.3(2) K from the peak in $\chi_c(T)$, in agreement with a peak in the zero-field heat capacity (Figure S4, Supporting Information).

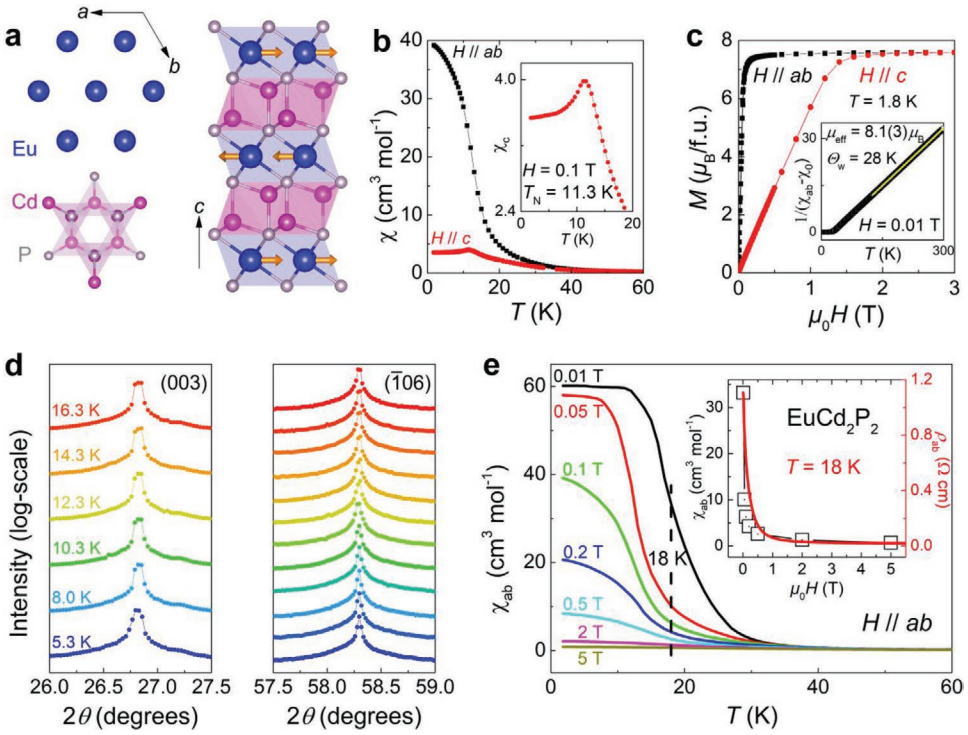

Figure 2. a) Trigonal lattice of $EuCd_2P_2$ made of triangular layers of Eu and Cd with octahedral and tetrahedral coordinations, respectively. A magnetic unit cell is illustrated with A-type AFM order. b) Magnetic susceptibility as a function of temperature in both the in-plane (black) and out-of-plane (red) fields. The inset determines $T_N = 11.3(2)$ K. c) Magnetization as a function of both in-plane (black) and out-of-plane (red) fields. The inset determines both the effective moment μ_{eff} and Weiss temperature Θ_W from a Curie-Weiss analysis (see also Figure S5, Supporting Information). d) High-resolution synchrotron diffraction data are collected for two Bragg peaks, (003) and ($\bar{1}$06), at different temperatures. There is no indication of a lattice distortion at T_N. e) Magnetic susceptibility as a function of temperature at several fields. The inset compares the field dependence of $\chi(T = 18\ K)$ and $\rho(T = 18\ K)$.

A combination of magnetization and X-ray data confirm that the CMR in $EuCd_2P_2$ is unrelated to either heterovalency or JT distortions, unlike in manganates. Figure 2c establishes a fixed Eu^{2+} oxidation state ($4f^7$ configuration), since both the saturated magnetization at low-T (7.6(6) μ_B) and the effective moment from a Curie-Weiss fit at high-T (8.1(3) μ_B) are consistent with the expected values for Eu^{2+} (7 and 8 μ_B, respectively). Note that the expected effective moment for Eu^{3+} ($4f^6$) is zero, hence we rule out a mixed valence of Eu^{2+}/Eu^{3+} unambiguously. In addition to the magnetization data, an analysis of the X-ray absorption spectroscopy in Figure S6, Supporting Information directly confirms the Eu^{2+} oxidation state without a mixed valence. Next, we used synchrotron X-rays to trace the temperature dependence of two representative diffraction peaks, (003) and ($\bar{1}$06), in Figure 2d. There is no abrupt shift or splitting of either peak as the temperature is varied through $T_N = 11.3$ K, hence we rule out a structural distortion (see also Figure S7, Supporting Information).

Considering the absence of both heterovalency and lattice distortions in $EuCd_2P_2$, the mechanism of CMR in this material must be different from that of the manganates.[2,8,9] As noted earlier, the CMR in $EuCd_2P_2$ is maximum at $1.5T_N$ and disappears either below T_N or above $5T_N$. This is the first indication that the magnetic fluctuations above T_N are related to CMR. The rapid suppression of $\chi(T)$ with field in Figure 2e confirms the presence of strong magnetic fluctuations that are suppressed by field. We make a cut through the $\chi(T)$ curves at $T = 18$ K, where CMR is maximum, and compare the field dependence of $\chi(18\ K)$ and $\rho(18\ K)$ in the inset of Figure 2e. The parallel behavior between $\chi(18\ K)$ and $\rho(18\ K)$ suggests that the suppression of magnetic fluctuations with field is responsible for the CMR in this material. Such spin fluctuations are consistent with recent theoretical work on $EuCd_2As_2$ which has a similar layered structure as $EuCd_2P_2$ where the spins are confined within the 2D Eu layers (Figure 2a).[28]

A more direct evidence for the spin fluctuations as the mechanism of CMR in $EuCd_2P_2$ comes from the AC susceptibility data in **Figure 3**. Two peaks are observed in the imaginary component $\chi''_{ac}(T)$. The lower temperature peak coincides with the AFM peak in the DC susceptibility (Figure 2b), but the higher temperature peak does not have any counterpart in the DC data, that is, it can be regarded as a direct evidence of magnetic fluctuations. Remarkably, a small DC field of 0.5 T is enough to suppress this peak, similar to the rapid suppression of the resistivity peak at 18 K (Figure 1a). Therefore, a direct link is established between the peak from magnetic fluctuations in $\chi''_{ac}(T)$ and the peak in $\rho(T)$. We also provide scanning SQUID microscopy[29] images in Figure 3 to confirm the bulk measurements. The bright and dark images correspond to the peaks and valleys in the bulk $\chi''_{ac}(T)$ data. The images highlight spatial uniformity of the AC susceptibility and confirm the intrinsic origin of the magnetic fluctuations. Although our data are consistent with spin fluctuations as the source of CMR in $EuCd_2P_2$, other mechanisms such as band structure reconstruction and topological effects are also relevant to this material.[24,32]

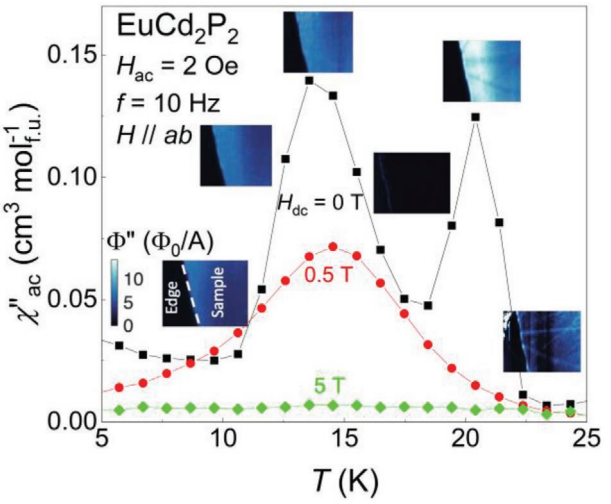

Figure 3. The imaginary component of the AC susceptibility data from a bulk sample is obtained at zero-field (black) as well as 0.5 and 5 T (red and green). The peaks at 13 and 20 K are due to the AFM order and fluctuations, respectively. The latter peak is suppressed with a small magnetic field similar to the CMR behavior. Zero-field scanning SQUID images with the size of 220×205 μm^2 are compared to the bulk data at crests and troughs. The streaks in the image are due to surface roughness.

The A-type AFM order in $EuCd_2P_2$ resembles a magnetic tunnel junction (MTJ)[30,31] as illustrated in the inset of **Figure 4**a. A consequence of such a magnetic structure is that CMR reaches -10^4% when the electric current is out of plane ($J \| c \rightarrow \rho_c$) and becomes even larger than the -10^3% effect with in-plane current ($J \| ab \rightarrow \rho_{ab}$). At 5 T MR is −28 000% when $J \| c$ and −7600% when $J \| ab$, in the same sample (inset of Figure 4a). It is noteworthy that the enormous -10^4% CMR in a crystal of $EuCd_2P_2$, grown inside a hot crucible without any optimization, is three times larger than in optimized samples of $La_{0.60}Y_{0.07}Ca_{0.33}MnO_x$.[21] We point out that the magnitude of CMR is nearly independent of the field direction regardless of whether the electric current is in-plane (Figure 1d) or out-of-plane (Figures S8 and S9, Supporting Information). The relation between CMR and magnetic fluctuations is highlighted in Figure 4b that shows the zero-field ρ_c is ten times larger than ρ_{ab} in the region of magnetic fluctuations (the red area). In contrast, ρ_c is only two times larger than ρ_{ab} in both the bad metal regime at high-T (yellow) and the ordered regime at low-T (blue).

Additional insight into the physics of $EuCd_2P_2$ comes from a comparison between three $EuCd_2X_2$ compounds with X = P, As, and Sb. One expects that the smaller spatial extension of the p-orbitals, from Sb (5p) to As (4p) and P (3p), reduces the coupling between the Eu and Cd layers and enhances the magnetic fluctuations, leading to a larger CMR. This is confirmed

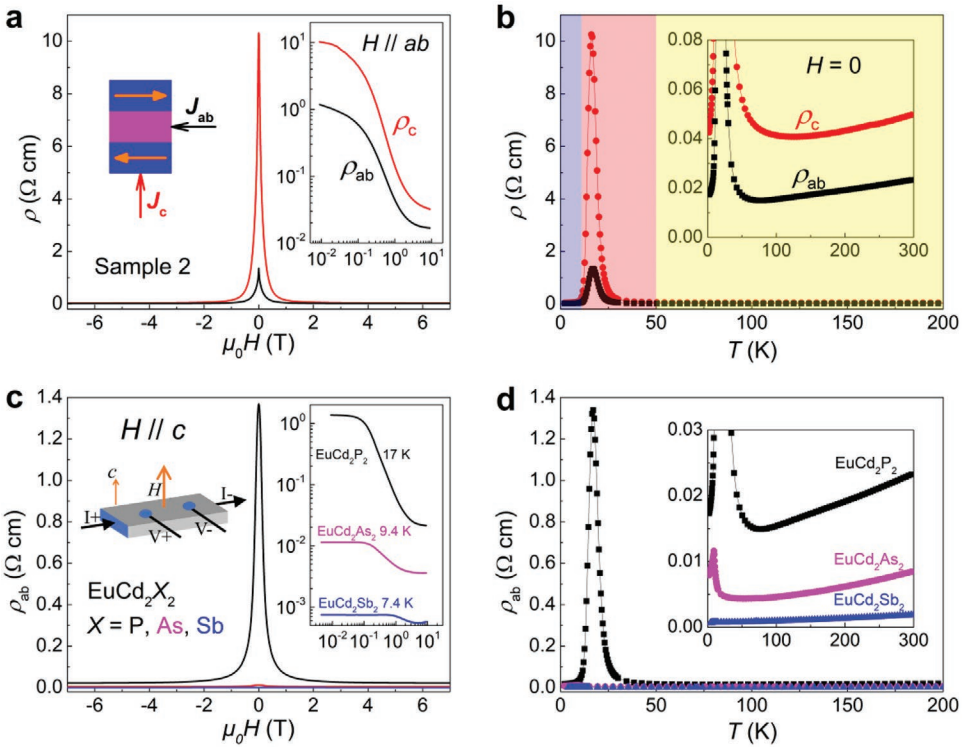

Figure 4. a) CMR in $EuCd_2P_2$ is one order of magnitude larger when the electric current is out-of-plane compared to in-plane. The left inset shows that each unit cell of $EuCd_2P_2$ resembles a MTJ. The right inset shows changes of ρ_c and ρ_{ab} in the log-scale. The data in this figure are from Sample 2, but the data in Figures 1 and 2 are from Sample 1. b) The magnitude of ρ_{ab} and ρ_c are comparable below T_N (blue region) and in the bad metal regime (yellow), but they are an order of magnitude apart in the region of magnetic fluctuations (red). c) Field dependence of resistivity in $EuCd_2P_2$ (black) compared to $EuCd_2As_2$ (magenta), and $EuCd_2Sb_2$ (blue). d) The colossal resistivity peak at low temperatures in $EuCd_2P_2$ makes the other two materials invisible. Inset: the room temperature resistivity increases from 2 mΩ cm in $EuCd_2Sb_2$ to 8 mΩ cm in $EuCd_2As_2$ and 23 mΩ cm in $EuCd_2P_2$.

in Figure 4c where CMR increases from −10% in $EuCd_2Sb_2$ to -10^2% in $EuCd_2As_2$, and -10^3% in $EuCd_2P_2$ (with $J \| ab$). Simultaneously the exchange correlations are expected to grow from X = Sb to As and P, leading to an increase in T_N from 7 to 9 and 11 K, respectively.[23–25] The buildup of correlations is evident in Figure 4d where both the violation of the Ioffe-Regel limit ($\rho > 1$ mΩ cm) in the bad metal regime (inset) and the resistivity peak near T_N are dramatically enhanced by replacing Sb with As and P.

To summarize, we have shown that $EuCd_2P_2$ exhibits a CMR that reached -10^4% due to strong magnetic fluctuations despite the absence of mixed valence and lattice distortions. Prior attempts to establish CMR without mixed valence has led to a much smaller effect, between −20 and −250%, for example, in $TlMn_2O_7$ (pyrochlore),[11] $FeCr_2S_4$ (spinel),[12] and $(Eu,Yb)_{14}MnSb_{11}$ (Zintl compounds).[13,14] The CMR values of these materials are summarized in **Table 1** and compared to $EuCd_2P_2$. Recently, a larger CMR of about −300% has been found in the Zintl compound $EuIn_2P_2$, which is also a layered material with hexagonal lattice ($P6_3/mmc$).[32] We believe that in this material, similar to $EuCd_2P_2$, CMR results from the layered structure and magnetic fluctuations although band structure and topological effects are also plausible mechanisms. However, due to In-In bonds within the layers, the magnetic anisotropy and the bad metal behavior are less prominent in $EuIn_2P_2$, as evident from a slow saturation of the in-plane magnetization and a resistivity of 2 mΩ cm at room temperature.[32] The absence of direct Cd-Cd bonds in the structure of $EuCd_2P_2$ seems to be beneficial to the CMR.

Due to its layered structure, intermetallic composition, and stability in air, $EuCd_2P_2$ is suitable for the fabrication of low temperature magnetic sensing and read/write devices. For example, lithographic techniques can be used to produce microscale spintronic devices from the single crystals. Since CMR is large regardless of the field direction (Figure 1d and Figure S9, Supporting Information), $EuCd_2P_2$ is convenient to work with, as the field does not need to be orientated along a specific crystallographic direction for the desired effect. Epitaxial techniques can be used to fabricate thin films and heterostructures from this layered compound for AFM spin torque and spin valve devices.[17,18] It is possible to even change the magnetic state of the material by altering the flux growth condition, as recently reported for $EuCd_2As_2$,[25] and to replace both Eu and Cd with other rare-earths and transition metals.[34] Future efforts in chemical doping, electrical biasing, and mechanical straining will enable tuning of the magnetic fluctuations, hence controlling the temperature/field regime of CMR in $EuCd_2P_2$ and its derivatives.

Table 1. Summary of the CMR values in several materials including oxides, chalcogenides, and pnictides.

Reference	Material	CMR value	Field [T]
[10]	$La_{0.75}Ca_{0.25}MnO_3$	−25%, −400%	1, 4
[11]	$TlMn_2O_7$	−200–250%	8
[12]	$FeCr_2S_4$	−25%	6
[13]	$Eu_{14}MnSb_{11}$	−66%	5
[14]	$Yb_{14}MnSb_{11}$	−20%	5.5
[32]	$EuIn_2P_2$	−298%	5
[33]	$EuIn_2As_2$	−143%	5
This work	$EuCd_2P_2$	-6×10^3% for $I \| ab$, -2.8×10^4% for $I \| c$	5

Experimental Section

Crystal Growth: Single crystals of $EuCd_2P_2$ were grown in Sn flux, by using sublimed ingots of europium (Alfa Aesar, 99.9%), cadmium tear drops (Alfa Aesar, 99.95%), red amorphous phosphorus powder (Alfa Aesar, 98.9%), and tin shots (Alfa Aesar, 99.999%) as the starting materials. Eu ingots were cut into small pieces and mixed with other elements with a mole ratio Eu: Cd: P: Sn = 1: 2: 2: 20. The mixture was then loaded into an alumina crucible inside an evacuated quartz ampule and slowly heated to 950 °C, held for 36 h, cooled to 550 °C at 3 °C/h, and finally centrifuged to remove the excess flux.

Transport, Heat capacity, and Magnetization Measurements: The electrical resistivity was measured with a standard four-probe technique using a Quantum Design Physical Property Measurement System (PPMS) Dynacool with a high-resolution rotator option. The heat capacity was measured using the PPMS with a relaxation time method on a carefully polished sample. A flat crystal (1.2 mg) was adopted to measure DC and AC magnetization using a Quantum Design Magnetic Property Measurement System (MPMS3).

X-Ray Diffraction: Synchrotron X-ray diffraction measurements were performed at the Advanced Photon Source at beamline 6-ID B using a PSI diffractometer. The single crystal sample was cooled with a 4 K ARS cryostat refrigerator. The diffraction matrix of the sample was aligned with the (003) and ($\bar{1}$06) reflections with an X-ray energy of 11.712 keV. Temperature dependence reflection angular position was monitored by realigning the sample at each temperature before the data was taken. The crystal structures of $EuCd_2P_2$ and $SrCd_2P_2$ were refined using the powder X-ray diffraction data obtained in house. A Bruker D8 ECO instrument was used with 40 keV copper source and a 1D LYNXEYE XE detector and the FullProf suite was used for the structural refinements.

X-Ray Absorption: X-ray absorption data were collected at beamline 4-ID-D of the Advanced Photon Source at Argonne National Laboratory. The measurements were done on a finely ground powder sample with total thickness optimized for transmission geometry. The samples were cooled in ^{4}He vapor using the variable temperature insert of a superconducting magnet. Data were collected across the magnetic ordering temperature, both in zero field and $H = 2$ T applied field.

Supporting Information

Supporting Information is available from the Wiley Online Library or from the author.

Acknowledgements

The authors thank M. Frith, Z.-X Shen, and T. Devereaux for helpful discussions. The work at Boston College was funded by the National Science Foundation under Award No. NSF/DMR-1708929. The work performed at the Advanced Photon Source was supported by the U.S. Department of Energy, Office of Science, and Office of Basic Energy Sciences under Contract No. DE-AC02-06CH11357. I.S. thanks the US DOD for partial support.

Conflict of Interest

The authors declare no conflict of interest.

Data Availability Statement

Research data are not shared.

Keywords

antiferromagnetism, colossal magnetoresistance, magnetic fluctuations, spintronics

Received: August 24, 2020
Revised: January 7, 2021
Published online: January 29, 2021

[1] A. P. Ramirez, *J. Phys. Condens. Matter* **1997**, *9*, 8171.
[2] H. Röder, J. Zang, A. R. Bishop, *Phys. Rev. Lett.* **1996**, *76*, 1356.
[3] E. Dagotto, *Science* **2005**, *309*, 257.
[4] M. B. Salamon, M. Jaime, *Rev. Mod. Phys.* **2001**, *73*, 583.
[5] J. M. D. Coey, M. Viret, S. v. Molnár, *Adv. Phys.* **1999**, *48*, 167.
[6] H. Y. Hwang, S.-W. Cheong, P. G. Radaelli, M. Marezio, B. Batlogg, *Phys. Rev. Lett.* **1995**, *75*, 914.
[7] I. Solovyev, N. Hamada, K. Terakura, *Phys. Rev. Lett.* **1996**, *76*, 4825.
[8] A. J. Millis, P. B. Littlewood, B. I. Shraiman, *Phys. Rev. Lett.* **1995**, *74*, 5144.
[9] A. J. Millis, *Nature* **1998**, *392*, 147.
[10] P. Schiffer, A. P. Ramirez, W. Bao, S.-W. Cheong, *Phys. Rev. Lett.* **1995**, *75*, 3336.
[11] M. A. Subramanian, B. H. Toby, A. P. Ramirez, W. J. Marshall, A. W. Sleight, G. H. Kwei, *Science* **1996**, *273*, 81.
[12] A. P. Ramirez, R. J. Cava, J. Krajewski, *Nature* **1997**, *386*, 156.
[13] J. Y. Chan, S. M. Kauzlarich, P. Klavins, R. N. Shelton, D. J. Webb, *Chem. Mater.* **1997**, *9*, 3132.
[14] I. R. Fisher, T. A. Wiener, S. L. Bud'ko, P. C. Canfield, J. Y. Chan, S. M. Kauzlarich, *Phys. Rev. B* **1999**, *59*, 13829.
[15] L. Smejkal, Y. Mokrousov, B. Yan, A. H. MacDonald, *Nat. Phys.* **2018**, *14*, 242.
[16] Y. Tokura, M. Kawasaki, N. Nagaosa, *Nat. Phys.* **2017**, *13*, 1056.
[17] J. Zelezny, P. Wadley, K. Olejník, A. Hoffmann, H. Ohno, *Nat. Phys.* **2018**, *14*, 220.
[18] H. Yan, Z. Feng, P. Qin, X. Zhou, H. Guo, X. Wang, H. Chen, X. Zhang, H. Wu, C. Jiang, Z. Liu, *Adv. Mater.* **2020**, *32*, 1905603.
[19] V. J. Emery, S. A. Kivelson, *Phys. Rev. Lett.* **1995**, *74*, 3253.
[20] S. Jin, T. H. Tiefel, M. McCormack, R. A. Fastnacht, R. Ramesh, L. H. Chen, *Science* **1994**, *264*, 413.
[21] S. Jin, H. M. O'Bryan, T. H. Tiefel, M. McCormack, W. W. Rhodes, *Appl. Phys. Lett.* **1995**, *66*, 382.
[22] M. McCormack, S. Jin, T. H. Tiefel, R. M. Fleming, J. M. Phillips, *Appl. Phys. Lett.* **1994**, *64*, 3045.
[23] J.-R. Soh, C. Donnerer, K. M. Hughes, E. Schierle, E. Weschke, D. Prabhakaran, A. T. Boothroyd, *Phys. Rev. B* **2018**, *98*, 064419.
[24] J.-Z. Ma, S. M. Nie, C. J. Yi, J. Jandke, T. Shang, M. Y. Yao, M. Naamneh, L. Q. Yan, Y. Sun, A. Chikina, V. N. Strocov, M. Medarde, M. Song, Y.-M. Xiong, G. Xu, W. Wulfhekel, J. Mesot, M. Reticcioli, C. Franchini, C. Mudry, M. Müller, Y. G. Shi, T. Qian, H. Ding, M. Shi, *Sci. Adv.* **2019**, *5*, eaaw4718.
[25] N. H. Jo, B. Kuthanazhi, Y. Wu, E. Timmons, T.-H. Kim, L. Zhou, L.-L. Wang, B. G. Ueland, A. Palasyuk, D. H. Ryan, R. J. McQueeney, K. Lee, B. Schrunk, A. A. Burkov, R. Prozorov, S. L. Bud'ko, A. Kaminski, P. C. Canfield, *Phys. Rev. B* **2020**, *101*, 140402.
[26] J.-R. Soh, E. Schierle, D. Y. Yan, H. Su, D. Prabhakaran, E. Weschke, Y. F. Guo, Y. G. Shi, A. T. Boothroyd, *Phys. Rev. B* **2020**, *102*, 014408.
[27] I. Schellenberg, U. Pfannenschmidt, M. Eul, C. Schwickert, R. Pöttgen, *Z. Anorg. Allg. Chem.* **2011**, *637*, 1863.
[28] M. C. Rahn, J.-R. Soh, S. Francoual, L. S. I. Veiga, J. Strempfer, J. Mardegan, D. Y. Yan, Y. F. Guo, Y. G. Shi, A. T. Boothroyd, *Phys. Rev. B* **2018**, *97*, 214422.
[29] I. Sochnikov, L. Maier, C. A. Watson, J. R. Kirtley, C. Gould, G. Tkachov, E. M. Hankiewicz, C. Brüne, H. Buhmann, L. W. Molenkamp, K. A. Moler, *Phys. Rev. Lett.* **2015**, *114*, 066801.
[30] S. Yuasa, T. Nagahama, A. Fukushima, Y. Suzuki, K. Ando, *Nat. Mater.* **2004**, *3*, 868.
[31] S. A. Wolf, D. D. Awschalom, R. A. Buhrman, J. M. Daughton, S. von Molnár, M. L. Roukes, A. Y. Chtchelkanova, D. M. Treger, *Science* **2001**, *294*, 1488.
[32] J. Jiang, S. M. Kauzlarich, *Chem. Mater.* **2006**, *18*, 435.
[33] A. M. Goforth, P. Klavins, J. C. Fettinger, S. M. Kauzlarich, *Inorg. Chem.* **2008**, *47*, 11048.
[34] K. Guo, Q. Cao, J. Zhao, *J. Rare Earths* **2013**, *31*, 1029.

